Supplementary Information (SI) for Journal of Materials Chemistry A.
This journal is © The Royal Society of Chemistry 2025

Supporting Information

Polymer binder with amine-facilitated lithium-ion transfer enabling high-loading silicon-based anodes

*Mengyao Zhu[a], Shengfei Wang[a], Shu Chen[a], Huajing Li[a], Xiangcheng Pan[a], Peng Gao[b], Xue Chen[b], Tao Wang[b], Guo Ji[b] and Yue Gao[a]**

Experimental Section: In this study, the polyacrylic acid (PAA), n-(2-aminoethyl) piperazine (AEP), were obtained from Dow Chemical Company. 1-ethyl-3-(3-dimethylaminopropyl) carbodiimidehydrochloride (EDC), N-hydroxy succinimide (NHS) and lithium hydroxide (LiOH) were purchased from Adamas. The commercial SiO materials were provided by Liyang Zichen New Material Technology Co., Ltd for the study and this commercial SiO material. CNT was purchased from Haiyi Co., Ltd. All other chemicals were of analytical grade and all solvents were purchased from Shanghai Chemical Reagent Co., Ltd without further treatment.

Synthesis of binder PAA-AEP: The PAA (1.50 g) was added to distilled water (150 mL), and adjusted with 1 M HCl and 1 M NaOH to adjust the pH to 5~6, subsequently EDC (2.00 g) and NHS (0.75 g) were added to the solution. The solution was stirred for one hour at room temperature. Then, n-(2-aminoethyl) piperazine (AEP) (0.34 g) was slowly added to the solution. The reaction solution was stirred for 12 h at room temperature, and the pH was maintained at 5.5 with 1 M HCl and 1 M NaOH during the reaction. After the reactant was purified by dialysis in distilled water for 48 h, the final product was obtained by freeze-dry.

Characterization: Fourier transform infrared spectrometer (FTIR) spectra were recorded on a Nicolet 6700 spectrometer (Thermo Fisher) in the range of 400-4000 cm^{-1} with the appropriate ATR accessory 64 times. The resolution of the spectra was 4 cm^{-1}. Rheological characterization of binder solutions was conducted at 25 ℃ using a TA Instruments model Discovery HR-3 rheometer equipped with a cone-plate geometry that had a cone diameter of 20 mm. The Raman mapping was made by Renishaw. The mapping area was 5×30 μm^2, and Raman spectra of 150

points (5-by-30 points) were recorded. After the 10th charge-discharge cycle, the Si thick-film electrodes were separated from the coin cells and washed with dimethyl carbonate (DMC) to remove the residual electrolyte, after which they were dried in the glovebox at room temperature. The Raman map in Figure 2a was generated by plotting the band with the maximum intensity at a frequency of 479 cm^{-1}. Gel permeation chromatography (GPC) plots were recorded on the Agilent 1260 instrument. Each sample was tested three times to ensure accuracy. The argon ion etching-assisted X-ray photoelectron spectroscopy (XPS) was collected using an ESXCALAB Xi^+ X-ray photoelectron spectrometer excited by monochromatic Al (1486.7 eV, 240 W) source. Before characterizations, all the samples were rinsed with dimethyl carbonate (DMC) three times and dried under a vacuum to remove the residual lithium salts and solvent. Mechanical tests were conducted on rectangular samples (typical dimensions: 30 mm × 5mm × 3 mm). The mechanical properties of the polymers were measured using an Instron 3343 machine in standard stress/strain experiments, the tensile curves were measured at a constant speed of 100 mm min^{-1}. Scanning electron microscope (SEM) images were taken on a Zeiss Gemini SEM500 FESEM scanning electron microscope. Before SEM tests of electrodes, batteries were disassembled in an argon-filled glovebox and then gently rinsed with diethyl carbonate (DEC) to remove the residual salts.

Electrochemical Characterization: The SiO anodes were fabricated by coating homogeneous mixed slurries, containing active material (80 wt.%), super P (10 wt.%), binder (5 wt.%) and CNT (2 wt.%), onto the copper collector. After drying the electrodes at 80 °C for 8 h to remove the solvent under vacuum, the mass loadings of electrodes (Φ12 mm) were approximately 1.5 mg cm^{-2}. The prepared electrodes were assembled into the CR2032 cells in an Argon-filled glove box (H_2O and O_2 < 1.0 ppm) using a Celgard 2325 separator. 1.0 M $LiPF_6$ in a mixture of ethylene carbonate and diethyl carbonate (EC/DEC, 1:1 by volume) containing 10 vol% fluoroethylene carbonate was used as the electrolyte, and 80 μL electrolyte was added to each coin cell. The capacity was calculated based on the mass loading of active material of the electrode. The galvanostatic charge/discharge tests were performed on Neware battery testers (Shenzhen, China) in a voltage range of 0.01–1.5 V for half-cell. SiO|NCM811 pouch cells were assembled by sandwiching the separator (Celgard 2400) between SiO anode and NMC811 cathode (Areal capacity=4.5 mAh cm^{-2}). The cathode composition is $LiNi_{0.8}Co_{0.1}Mn_{0.1}O_2$ (NCM811): Super P: PVDF=92:4:4. The N/P ratio of the SiO|NCM811 pouch cell is 1.05. 0.5 mL electrolyte was added to each pouch cell. The dimension of cathode is 2*3 cm^2, the dimension of anode is 2.05*3.05 cm^2. Full cell formation was performed by cycling between 2.8 V to 4.3V at 0.05 C rate and 0. 1 C rate. After that, the cell was cycled between 2.8 V to 4.3

V at 0.3 C rate. Cyclic voltammetry (CV) tests of the electrodes were measured on a CHI1000C electrochemical workstation in a voltage range of 0.01–1.5 V with different scanning rates of 0.05, 0.10, 0.15, 0.20, 0.30 and 0.50 mV s^{-1}. The AC impedance spectroscopy of cells at different cycles was conducted EC-Lab (ver. 13.40) software with a frequency range from 0.01 to 100 kHz. The GITT was recorded under a pulse current of 0.5 C for 15 min, followed by a relaxation period for 60 min. All the tests were performed at room temperature.

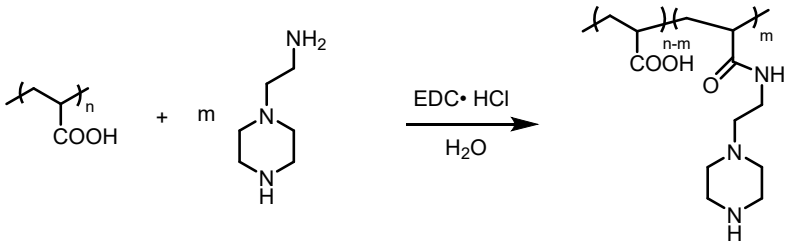

Figure S1. Formation route of PAA-AEP.

Sample	n(AA): n(AEP) (mol : mol)	Solid%
PAA-AEP1	5:1	1%
PAA-AEP2	8:1	1%
PAA-AEP3	20:1	1%

Table S1. The feeding ratio of the synthesis experiment.

Sample	C (%)	H (%)	N (%)
PAA-AEP1	52.80	8.87	13.4
PAA-AEP2	35.40	5.10	2.66
PAA-AEP3	49.13	11.30	13.88

Table S2. Elemental analysis of PAA-AEP.

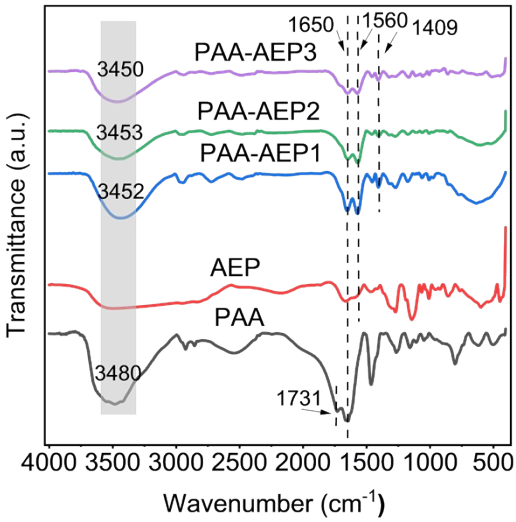

Figure S2. FTIR spectra of PAA, AEP, and PAA-AEP.

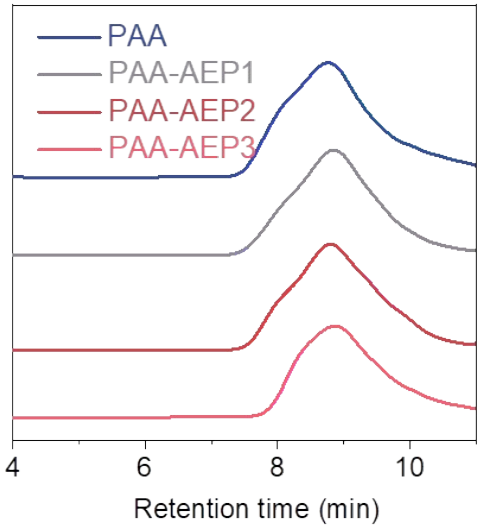

Figure S3. GPC elution trace of PAA and PAA-AEP.

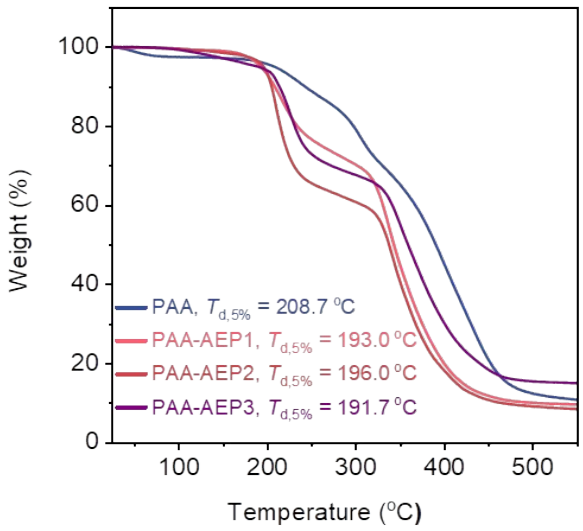

Figure S4. The TGA curve of PAA and PAA-AEP.

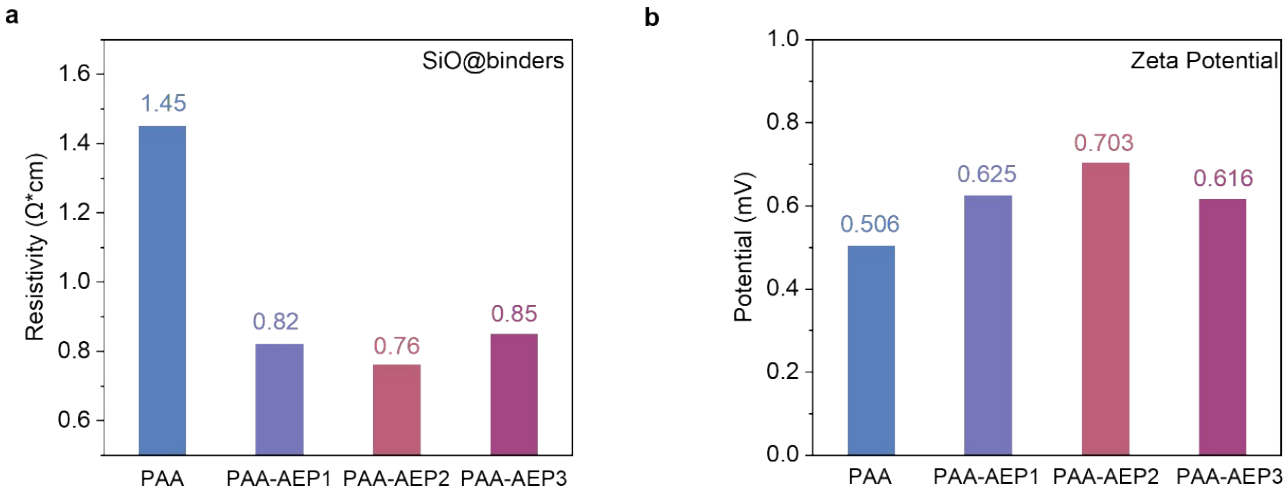

Figure S5. (a) The resistivity of SiO@PAA and SiO@PAA-AEP. (c) The zeta potential of SiO@PAA and SiO@PAA-AEP.

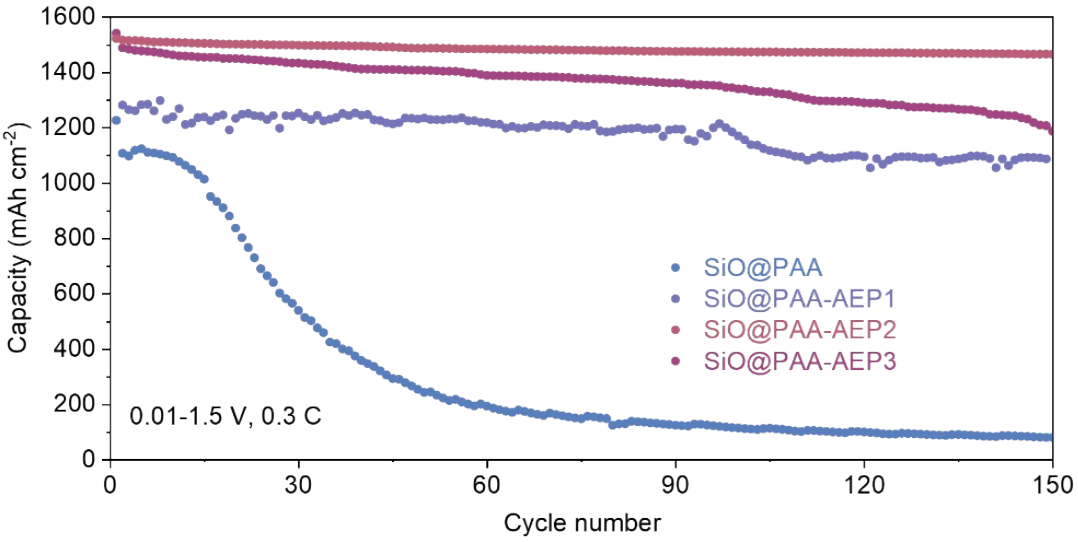

Figure S6. Cycling performances of the half cells with PAA, PAA-AEP1, 2, and 3 binders.

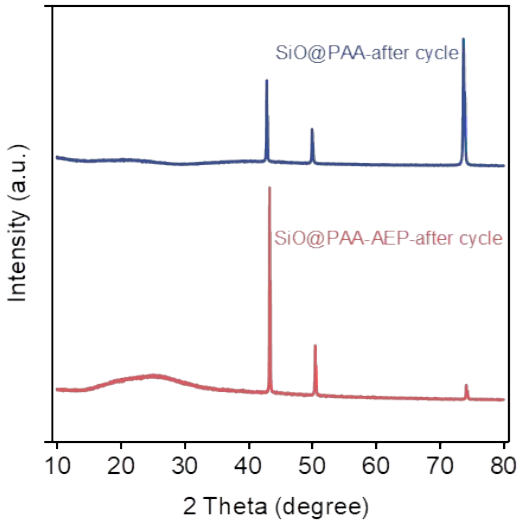

Figure S7. XRD curve of silicon anode with PAA and PAA-AEP.

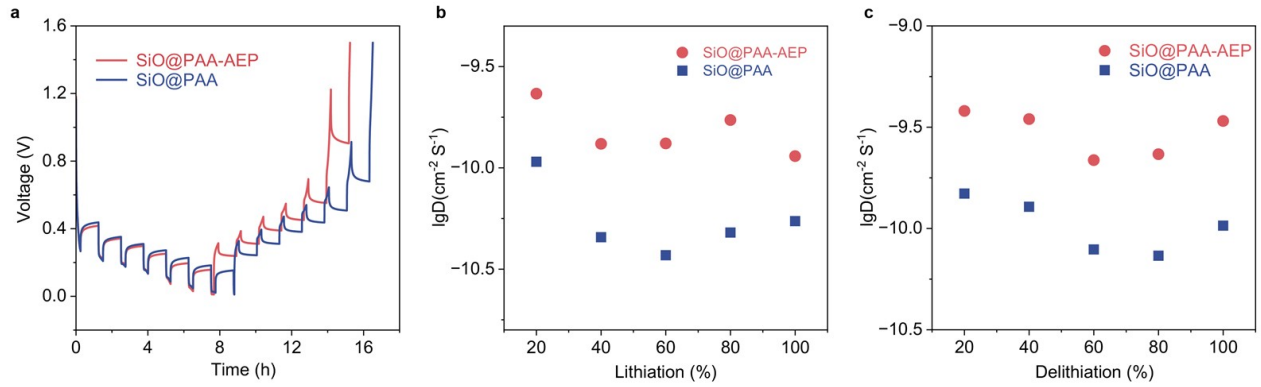

Figure S8. (a) GITT profiles of the SiO@PAA and SiO@PAA-AEP electrodes. (b,c) The diffusion coefficients of lithium ions for SiO@PAA and SiO@PAA-AEP during the lithiation and delithiation processes.

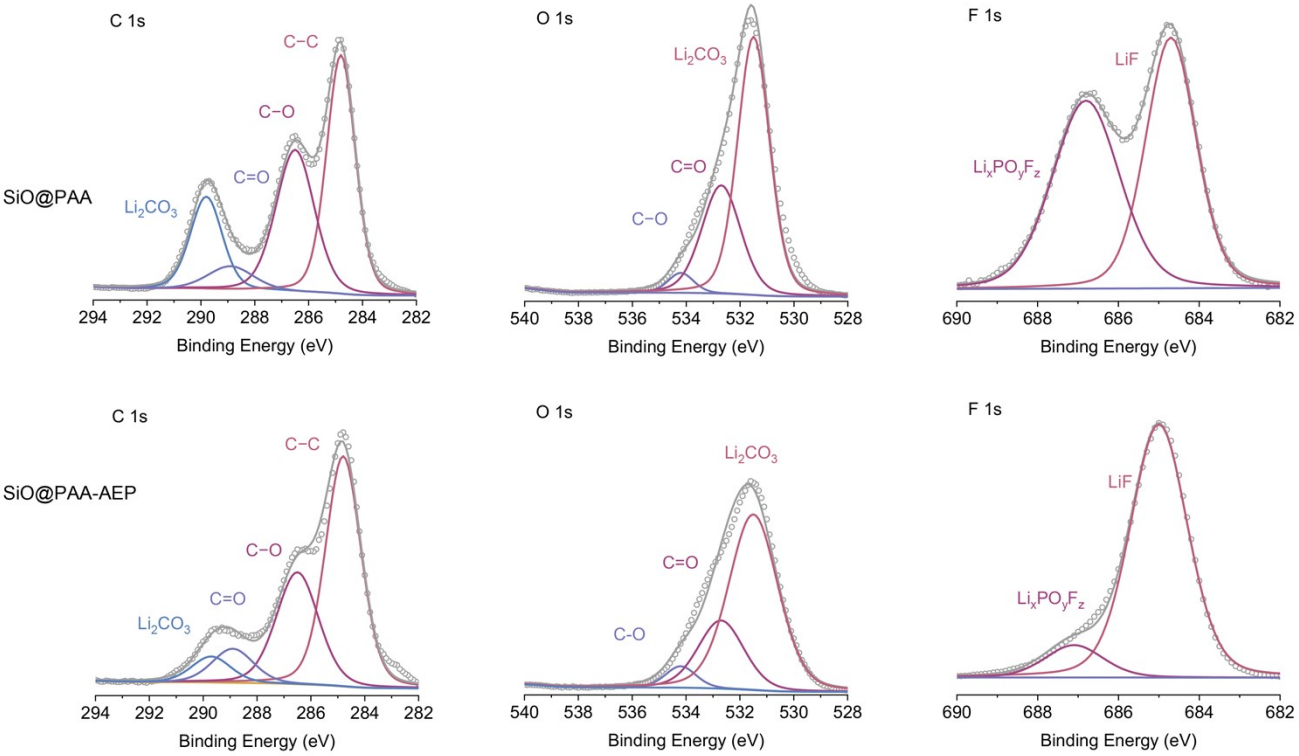

Figure S9. XPS spectra of SiO electrode with PAA and PAA-AEP binder in C 1s, O 1s and F 1s branches after the initial cycle at 0.05 C.

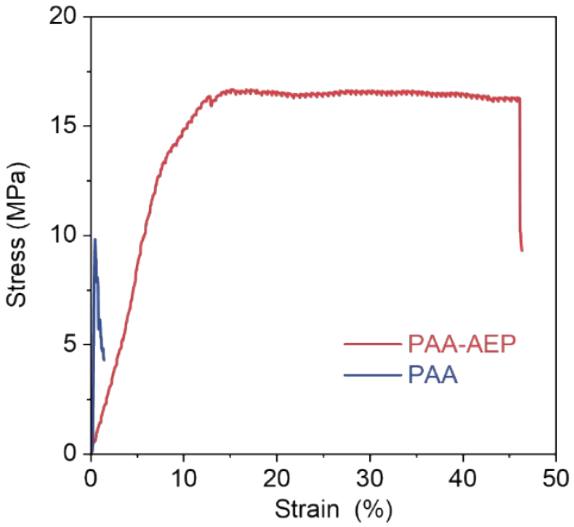

Figure S10. Stress-strain curves of PAA-AEP and PAA polymer film.

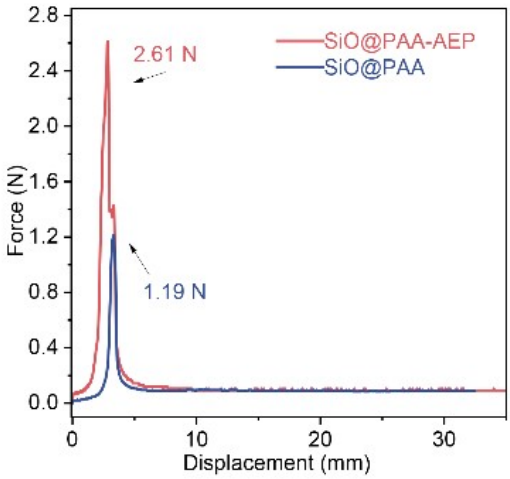

Figure S11. 180° peeling profiles of thin SiO electrodes with PAA and PAA-AEP (Loading: 1 mg cm^{-2}).

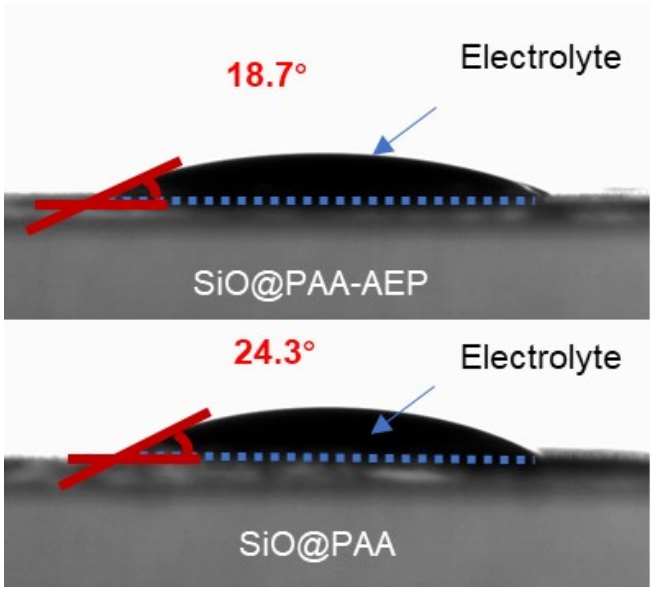

Figure S12. Digital photos for water contact angle of SiO composited with PAA and PAA-AEP binders.

Theory and method of DFT calculations

The quantum calculations of hydrogen bonds are referenced from Ref. 4 and Ref. 5 The hydrogen bond dissociation energy ($^{\Delta E_{HB}}$) is defined as:

$\Delta E_{HB} = E_{complex} - E_D - E_A + E_{BSSE}$

Where $^{E_{complex}}$, ^{E_D} and ^{E_A} are the energy of the complex, the donor and acceptor in the gas phase, respectively.$^{E_{BSSE}}$ is the basis set superposition error, which is typically necessary when calculating weak interactions.

For species m, the energy is given by:

$E_m = E_{electron} + ZPVE$

Where $^{E_{electron}}$ is the electronic energy of species m, and ^{ZPVE} is the zero-point vibrational energy.

DFT calculations were performed using the Gaussian 16 software package. The structure optimization and frequency calculations of the complex, donor, and acceptor were carried out at the B3LYP/6-311+G(d,p) level, with DFT-GD3BJ dispersion correction applied. Frequency calculations confirmed that each optimized geometry corresponds to a minimum on the potential energy surface with no imaginary frequencies. Zero-point vibrational energy were obtained from the frequency calculations. VMD software was used for molecular visualization and mapping.

Result and discussion

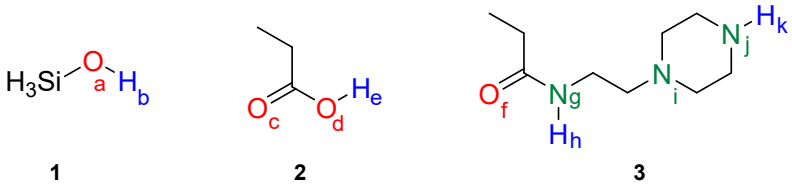

Figure S13. Three organic species were first set up to simulate the hydroxyl group on the silicon anode surface, the repeating unit of PAA and AEP.

The DFT calculation results are as follows (Table S3, Table S4 and Figure S14).

Complex	Donor	Acceptor	Bond Type	Bond length (Å)	Bond Angle (°)	BSSE (kcal/mol)	Bond Energy (kcal/mol)
4	1	2	OaHb—Od	1.99	2.52	0.871988023	0.353045523
5	1	3	OaHb—Of	1.79	12.81	0.994696652	-9.261728098
6	1	3	OaHb—Ni	1.76	3.02	1.735411449	-11.1654238

7	1	3	OaHb—Nj	1.78	2.78	1.049003943	-9.272492557
8	2	1	OdHe—Oa	1.78	9.26	0.901470084	-9.498212916
9	3	1	NgHh—Oa	1.95	6.93	1.379137581	-5.358769169
10	3	1	NjHk—Oa	2.09	3.61	0.900765145	-3.565277855

Tabel S3. DFT calculation result of hydrogen bonds.

Species	Energy (kcal/mol)
1	-230401.7471
2	-168427.9153
3	-372623.8734
4	-398830.1814
5	-603035.8769
6	-603038.5213
7	-603035.942
8	-398840.0621
9	-603032.3584
10	-603030.0866

Table S4. DFT calculation result of each species.

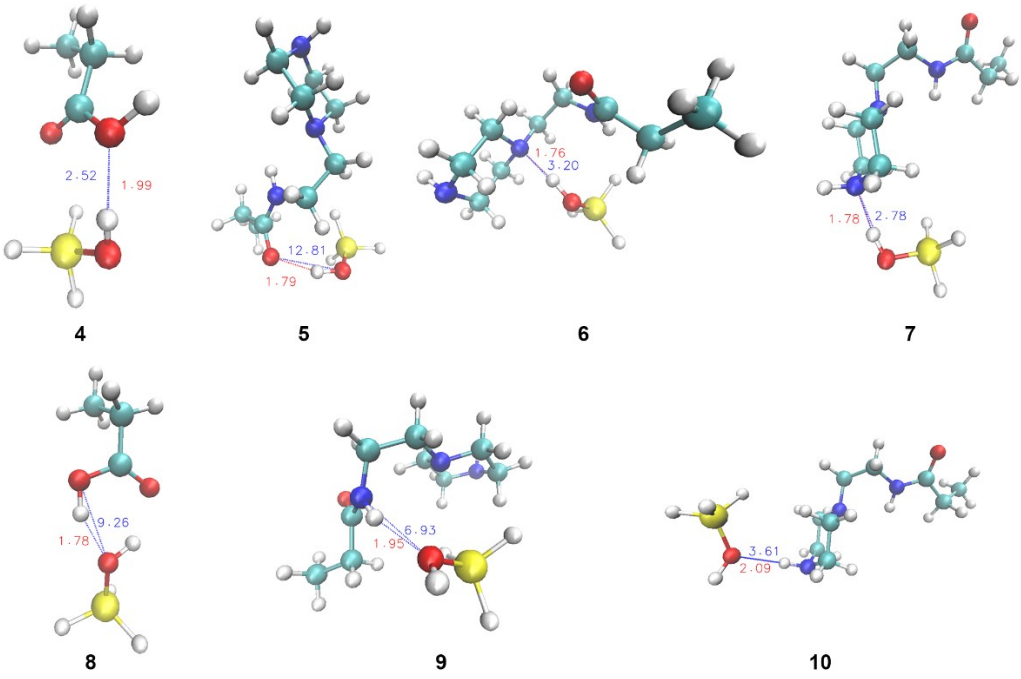

Figure S14. The structure of each complex. Red label is length(Å) of hydrogen bond. Blue label is angle(°) of hydrogen bond.

Summary

It is inferred that PAA mainly relies on the -COOH group as a donor to form hydrogen bonds with the hydroxyl group on the silicon surface, with a bond energy of -9.50 kcal mol^{-1}. When PAA copolymerizes with AEP, the introduced piperazine ring can provide the more electronegative nitrogen element, which acts as a hydrogen bond acceptor for the silicon hydroxyl group, with bond energies generally reaching -9 kcal mol^{-1}, and up to approximately -11.16 kcal mol^{-1}. At the same time, the N-H bond of the piperazine ring, as a donor, can form hydrogen bonds with a bond energy of around -5 kcal mol^{-1}. This gives the PAA-AEP copolymer more diverse hydrogen bonding sites and modes compared to the PAA homopolymer, thereby providing a stronger surface binding force.

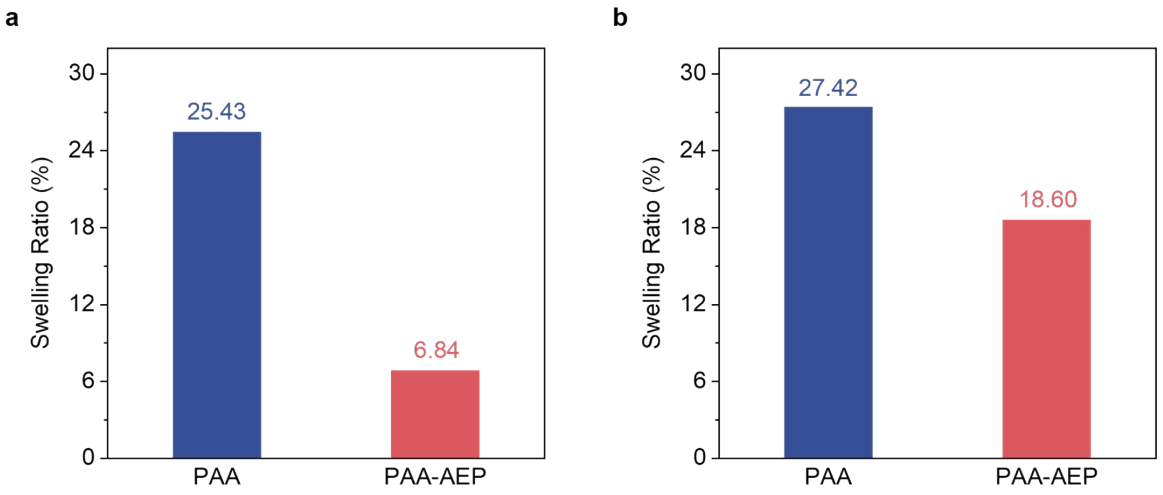

Figure S15. (a) The swelling ratio of binders soaked in electrolyte for 48 h. (b) The swelling ratio of binders soaked in electrolyte for 72 h.

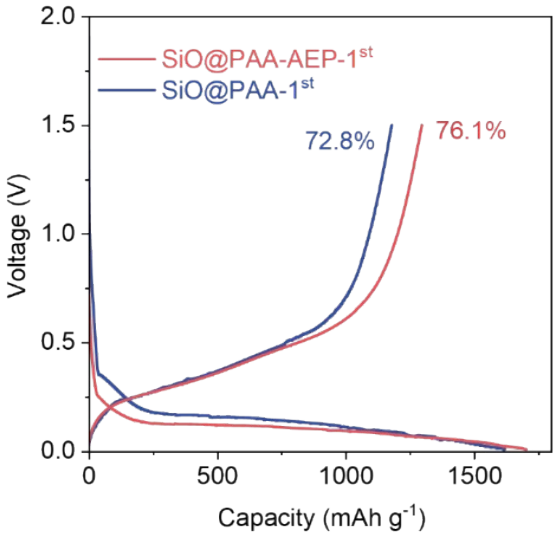

Figure S16. The initial coulombic efficiency of SiO@PAA-AEP electrode of the half cells in 1 mAh cm^{-2}.

Material	Li-ion transport site	Intial loading	Cycling stability	Reference
Si@AP	O	0.5 mAh cm^{-2}	83.9% after 100 cycles at 8 A g^{-1}	Adv. Energy Mater. 2022, 12 (29), 263
Si@PVA-PAA	O	0.5 mAh cm^{-2}	75.9% after 500 cycles at 1 C (1 C = 4.2 A g^{-1})	J. Mater.Chem. A 2021, 9 (13), 8416
SiO@HCS-PFM	O	4 mAh cm^{-2}	86.3% after 300 cycles	Nat Energy 2023, 8, 129
SiO@PFA-TPU	O	4 mAh cm^{-2}	60.0% after 100 cycles	ACS Enetgy Lett. 2021, 6, 290.
Si@β-CD	O	2 mAh cm^{-2}	85.41% after 50 cycles at 500 mA g^{-1}	Energy Environ. Mater. 2020, 4 (1), 72
Si@PAA-UPy	O	1 mAh cm^{-2}	62.89% after 110 cycles at 840 mA g^{-1}	Small 2018, 14, 29
SiO@PAA-AEP	**N**	**4.5 mAh cm^{-2}**	**89.0% after 700 cycles at 0.3C (1 C = 1400 mAh g^{-1})**	**This work**

Table S5. The performance comparison between this work and other binder structures reported in the literature.

REFERENCES

(1) Giubertoni, G., Sofronov, O.O. & Bakker, H.J. Effect Of Intramolecular Hydrogen-Bond Formation On The Molecular Conformation Of Amino Acids. *Commun Chem* **2020**, *3*, 84.

(2) Fedorova, I.V., Safonova, L.P. Comparisons of NH…O and OH…O Hydrogen Bonds in Various Ethanolammonium–Based Protic Ionic Liquids. *Struct Chem,* **2021**, *32*, 2061–2073.

(3) Weng, Z.; Di, S.; Chen, L.; Wu, G.; Zhang, Y.; Jia, C.; Zhang, N.; Liu, X.; Chen, G. Random Copolymer Hydrogel as Elastic Binder for the SiOx Microparticle Anode in Lithium-Ion Batteries. *ACS Appl. Mater. Interfaces* **2022**, *14*, 42494−42505.

(4) Hao, M.-H. Theoretical Calculation of Hydrogen-Bonding Strength for Drug Molecules. *J. Chem. Theory Comput.* **2006**, *2*, 863−872.

(5) Chai, K.; Lu, X.; Zhou, Y.; Liu, H.; Wang, G.; Jing, Z.; Zhu, F.; Han, L. Hydrogen Bonds in Aqueous Choline Chloride Solutions by DFT Calculations and X-ray Scattering. *J. Mol. Liquids* **2022**, *362*, 119742.

(6) Humphrey, W., Dalke, A. and Schulten, K., VM -Visual Molecular Dynamics. *J. Molec. Graphics* **1996**,*14.1*, 33-38.

(7) Hu, B.; Fan, H.; Li, H.; Ravivarma, M.; Song, J. Five-Membered Ring Nitroxide Radical: A New Class of High-Potential, Stable Catholytes for Neutral Aqueous Organic Redox Flow Batteries. *Adv. Funct. Mater.* **2021**, *31*, 2102734.

(8) Sun, J.; Liu, Y.; Cui, Y. Promises and Challenges of Nanomaterials for Lithium-Based Rechargeable Batteries. *Nat. Energy* **2016**, *1*, 16071.

(9) Cai, W.; Yao, Y. X.; Zhu, G. L.; Yan, C.; Jiang, L. L.; He, C.; Huang, J. Q.; Zhang, Q. A Review on Energy Chemistry of Fast-Charging Anodes. *Chem. Soc. Rev*. **2020**, *49*, 3806-3833.

(10) Fu, R.; Ji, J.; Yun, L.; Jiang, Y.; Zhang, J.; Zhou, X.; Liu, Z. Graphene Wrapped Silicon Suboxides Anodes with Suppressed Li Uptake Behavior Enabled Superior Cycling Stability. *Energy Stor. Mater*. **2021**, *35*, 317-326.

(11) Ryou, M. H.; Kim, J.; Lee, I.; Kim, S.; Jeong, Y. K.; Hong, S.; Ryu, J. H.; Kim, T. S.; Park, J. K.; Lee, H.; et al. Mussel-Inspired Adhesive Binders for High-Performance Silicon Nanoparticle Anodes in Lithium-Ion Batteries. *Adv. Mater.* **2013**, *25*, 1571-1576.

(12) Huang, Q.; Song, J.; Gao, Y.; Wang, D.; Liu, S.; Peng, S.; Usher, C.; Goliaszewski, A.; Wang, D. Supremely Elastic Gel Polymer Electrolyte Enables a Reliable Electrode Structure for Silicon-Based Anodes. *Nat. Commun.* **2019**, *10*, 5586